Peer-Reviewed Technical Communication

Geoacoustic Inversion of Airgun Data Under Influence of Internal Waves

Hefeng Dong, *Member, IEEE*, Mohsen Badiey, *Member, IEEE*, and N. Ross Chapman, *Fellow, IEEE*

***Abstract*—In this paper, broadband airgun data from the 1995 Shallow Water Acoustics in Random Media (SWARM'95) experiment are analyzed to study the influence of internal waves on sound propagation and modal behavior, and the subsequent effects on geoacoustic inversion. Modal behavior and fluctuation due to sound intensity focusing and defocusing, when the leading front of internal waves is parallel to and approaches or passes through the acoustic propagation track, are presented. A modal filtering technique, the time-warping transform, is applied to the airgun data to resolve dispersed modes. The extracted modes are used to estimate seabed model parameters by geoacoustic inversion. Two scenarios, defocusing and focusing periods containing 14 events, are selected for study. Seven data sets for each type (defocusing or focusing) are analyzed to extract dispersion curves and carry out geoacoustic inversion. The inversion results for each type of the events are similar with a small standard deviation from the mean. However, the mean values and standard deviations for the defocusing and focusing types are quite different. The impacts of internal waves on inversion results are presented and discussed.**

***Index Terms*—Defocusing and focusing, dispersion curves, geoacoustic inversion, internal waves, warping transform.**

I. Introduction

THE impact of ocean environmental variations on sound propagation in shallow water has received much attention in recent years. Of particular interest in this paper are the influence of internal waves on sound propagation and modal behavior and the consequent effects on geoacoustic inversion. Sound-field fluctuation due to internal waves in shallow-water regions and the influence of internal waves on sound propagation and sound intensity have been studied analytically, numerically, and experimentally [1]–[11]. Zhou *et al.* [1] first examined the frequency spectra variability in the Yellow Sea and recorded significant intensity decreases for specific frequencies. This was referred to as an "anomalous attenuation" and was reported as the result of resonant interactions between acoustic waves and the quasiperiodic spatial structure created by an internal solitary waves train propagating nearly parallel to the acoustic propagation direction. Sound intensity experiences focusing and defocusing fluctuations when the leading front of internal waves is nearly parallel to and passes through the source–receiver track. The interaction with the internal wave causes horizontal refraction, and sound energy is removed from the acoustic propagation plane [6], [9]–[12]. Furthermore, sound-speed fluctuations in the water column due to internal waves cause coupling between propagating acoustic modes.

Manuscript received February 6, 2016; revised July 12, 2016; accepted September 15, 2016. Date of publication October 19, 2016; date of current version July 12, 2017.

Associate Editor: Z.-H. Michalopoulou.

H. Dong is with the Department of Electronics and Telecommunications, Norwegian University of Science and Technology (NTNU), Trondheim 7491, Norway (e-mail: hefeng.dong@ntnu.no).

M. Badiey is with the College of Earth, Ocean, and Environment, University of Delaware, Newark, DE 19716 USA (e-mail: badiey@udel.edu).

N. R. Chapman is with the School of Earth and Ocean Sciences, University of Victoria, Victoria, BC V8W 3P6 Canada (e-mail: chapman@uvic.ca).

Digital Object Identifier 10.1109/JOE.2016.2611763

The effects of water column variability on geoacoustic inversion have been studied by several researchers [13]–[16]. Lin *et al.* [13] presented a method for evaluating the effect of water-column mismatch on geoacoustic inversion and tested for linear and nonlinear internal waves causing the water-column mismatch by numerical simulations. Becker and Frisk [14] studied the effect of the water-column variability on horizontal wave number estimation and geoacoustic inversion using synthetic data, and concluded that mode coupling is important even for weak internal waves but its effect on eigenvalue estimation is negligible, and model-based geoacoustic inversion is robust using a range averaged sound-speed profile. The ocean sound-speed profile was parameterized in terms of empirical orthogonal functions and inverted along with the geoacoustic parameters to account for the varying water-column environment [15]. However, the approach in [15] is not effective in environments with severe variation along the propagation path that could cause mode coupling.

In this paper, we present analysis of broadband acoustic signals to study the influence of internal waves on sound propagation, sound intensity and modal behavior, and the consequent effect on the results of geoacoustic inversion under different scenarios: defocusing and focusing events. The data were generated by an airgun source at a shallow depth and recorded by a vertical line array (VLA) in the 1995 Shallow Water Acoustics in Random Media (SWARM'95) experiment at a shallow-water region of the New Jersey Shelf. The airgun source provided high-quality long-range broadband data over a frequency band between 20 and 180 Hz. Modal behavior and fluctuation due to sound intensity focusing and defocusing are presented. A modal filtering technique, the time-warping transform, is used for time-frequency analysis to extract modal spectra and dispersion curves. Modal arrival times from the estimated dispersion curves with known source–receiver distance are used as input data for geoacoustic inversion to estimate seabed geoacoustic properties. The inversion results for the defocusing and focusing periods under the influence of internal waves are presented and discussed.

The remainder of this paper is organized as follows. Section II describes the experiment including oceanographic information. Section III presents time-frequency analysis and warping transform to resolve dispersion modes. Section IV presents inversion scheme and inversion results, and discussions on the influence of the internal waves on the inversion results between defocusing and focusing periods. Section V summarizes the work.

II. Description of the Experiments

The SWARM experiment was conducted at the Mid-Atlantic Bight on the continental shelf region off the coast of New Jersey in summer 1995 [5]. The data used in this paper were recorded in a sub-experiment between 19:00 and 20:00 GMT on August 4. The data were collected by a Woods Hole Oceanographic Institution (WHOI, Woods Hole, MA, USA) VLA with 16 hydrophones evenly

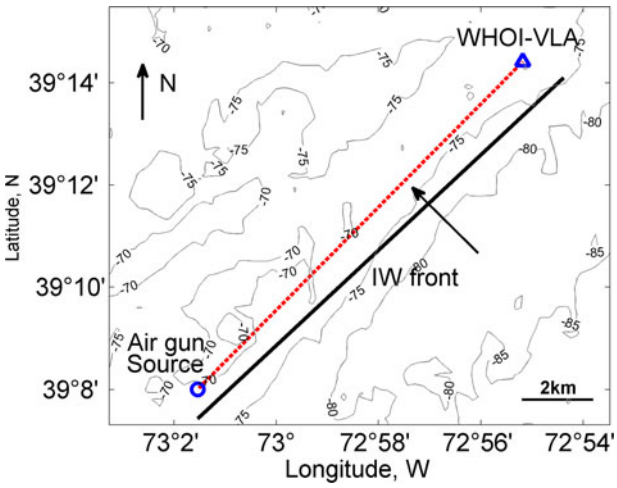

Fig. 1. Bathymetry map of the experimental site, acoustic propagation track (dashed line) and the IW front (solid line) reconstructed at 17:20:30 GMT.

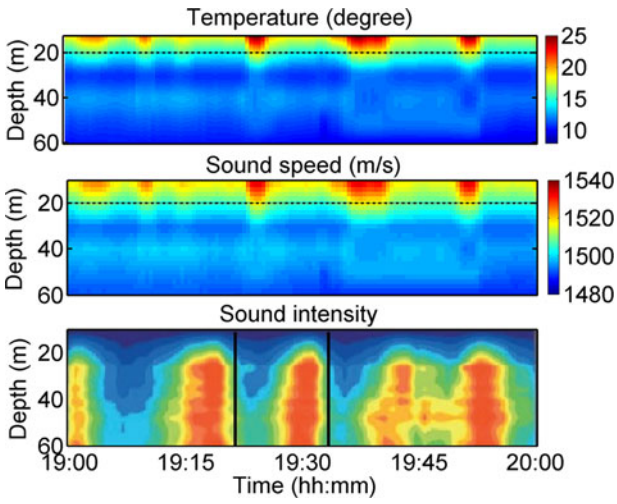

Fig. 2. (Top) Thermistor chain data between 19:00–20:00 GMT on August 4. (Middle) Sound-speed profiles generated from the thermistor chain data. (Bottom) Sound intensity (W/m^2) fluctuation during the same period and one cycle of the fluctuation denoted by the lines consisting of seven defocusing (e.g., 19:21–19:27) events and seven focusing (e.g. 19:28–19:34) events. Higher intensity is indicated by red shades.

spaced at 3.5 m from 14.9 to 67.4 m below the sea surface. The data were generated by an airgun source at 12 m below the sea surface and 15 km from the receiving array. The airgun source was fired at a rate of 1 min between shots. The water depth along the source–receiver track was almost constant around 72 m. Fig. 1 shows the bathymetry map of the experimental site, acoustic propagation track between the source and the VLA, and the internal wave (IW) front. A thermistor chain that spanned the water column at the VLA location was deployed to measure temperature variation during the experiment. The temperature was recorded every 30 s.

Fig. 2 plots the thermistor chain data (upper panel) between 19:00 and 20:00 GMT on August 4, and the sound-speed profiles generated from the thermistor data are shown in the middle panel. Badiey *et al.* [5] showed that during this period an internal wave packet was passing near the VLA through the acoustic propagation track. Due to the internal wave passage, the temperature recorded on the thermistor chain fluctuates near the water surface layer of 20–25 m and, as the depth increases, the temperature approaches a constant value. Moreover, it is observed that the temperature fluctuation has a period of approximately 12–15 min and the sound speed in the upper layer of the water column has large variation, which influences sound propagation and mode structure. Sound intensity influenced by internal waves experiences focusing and defocusing. The fluctuation of the sound intensity for the same period is shown in the bottom panel. Data sets in one cycle of sound intensity fluctuation denoted by the two lines in the plot are selected for study of modal behavior and geoacoustic inversion. There are 14 data sets in the cycle, seven data sets within the defocusing period (19:21–19:27) and seven data sets within the focusing period (19:28–19:34). Fig. 3 plots the sound-speed profiles during the seven defocusing events (solid curves) and seven focusing events (dashed curves). For the focusing events, the sound-speed profiles are very similar, while the sound-speed profiles for the defocusing events are different and large variation occurs in the upper layer of the water column, which influences the modal travel times, especially for the higher order modes. During the defocusing period mode amplitudes are reduced as sound energy from higher order modes and higher frequency components is removed out of the acoustic propagation plane. The situation presented in this paper is different from the cases studied in [14], [15], [17], and [18] where the majority of water-column variability occurs at midwater depths.

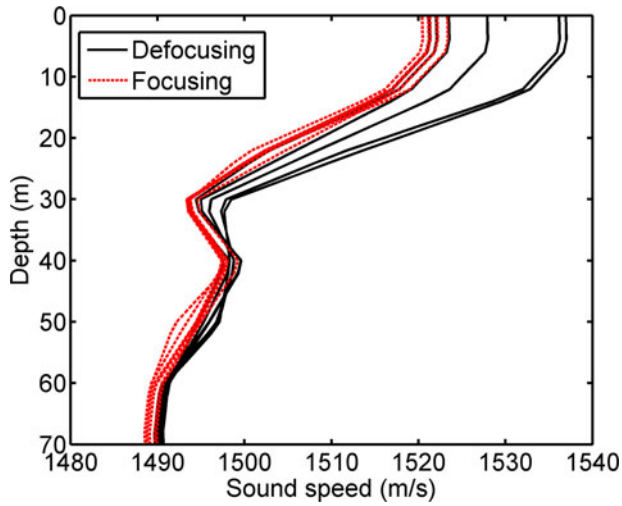

Fig. 3. Sound-speed profiles during the seven defocusing and seven focusing events denoted between the two lines in the bottom panel of Fig. 2.

III. Time-Frequency Analysis

The internal wave influences sound intensity and modal properties in frequency content, amplitude, and number of modes that can be resolved. Data received at the bottom hydrophone at 67.4 m below the sea surface are selected for the study. The envelopes of the received signals from the bottom hydrophone for the selected defocusing (left) and focusing (right) events are presented in Fig. 4. The signals are obtained using 10-Hz narrowband filters on the broadband signals with a carrier frequency of 60 Hz. Three modes are evident in this frequency band for both the defocusing and focusing events, and the sound intensity level of the second mode is strongest for the focusing events. However, the modal amplitudes of the defocusing events are weaker than those of the focusing events, and the sound intensity levels within the defocusing and focusing events are also different due to time variation of the oceanographic environment. Fig. 5 shows the spectra of the signals of the defocusing (upper) and focusing (bottom) events. In both plots several natural modulations are observed, which are due to the bubble pulse oscillations. The useful band is from 20 to

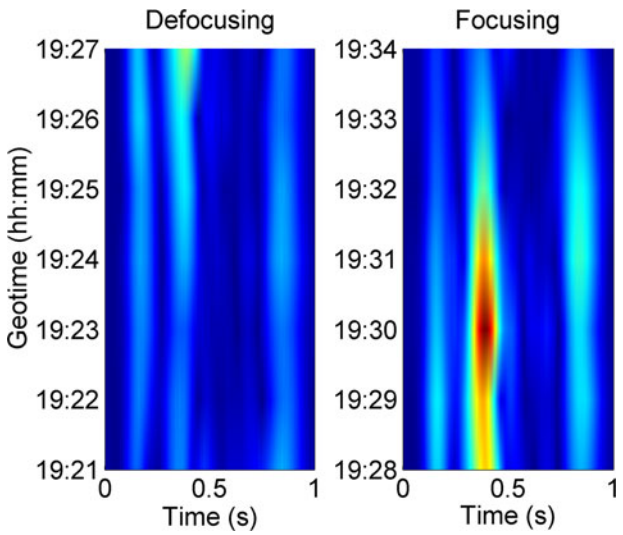

Fig. 4. Envelope of the received signals at the bottom most hydrophone as a function of geotime for the defocusing (left) and focusing (right) events. The same color scale is used for both plots, and warm colors represent large values.

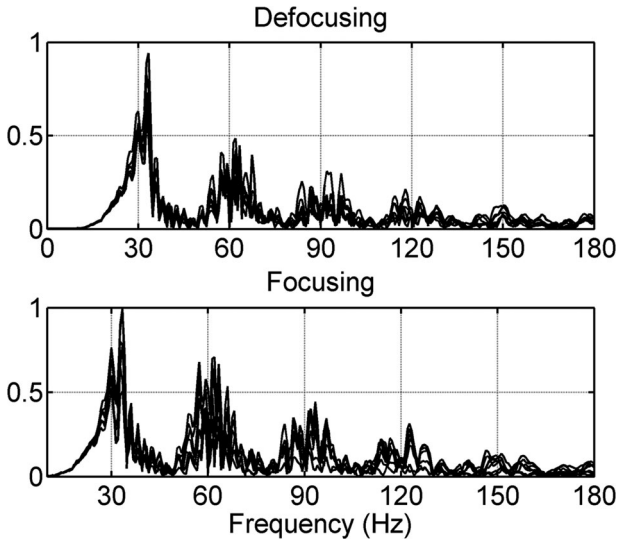

Fig. 5. Spectra of the received signals for the defocusing (upper) and focusing (bottom) events. The spectra are normalized by the same scale.

150 Hz and is separated into four sub-bands centered at 30, 60, 90, and 120 Hz. The bandwidth of each sub-band is quite narrow.

Time-frequency representations of the received signals for a defocusing event at 19:25:00 (left) and a focusing event at 19:31:00 (right) are presented in Fig. 6. The modal structures of the two events are similar, whereas the number of modes and sound intensity levels are different. There are three modes for the defocusing event and four modes for the forcusing event. However, the modes are not separated. The maximum sound intensity level of the forcusing event is around four times larger than that of the defocusing event. This phenomenon is due to horizontal refraction caused by internal wave solitons, which pulls the sound energy in and out of the source–receiver plane and leads to 3-D propagation [6], [9]–[12]. When the sound intensity experiences defocusing, the higher frequency components of higher order modes are reduced in strength due to the horizontal refraction, leading to significantly weaker signal strength in the highest order modes. The different modal behavior for different events and the different number of detected modes influence the overall depth penetration into the

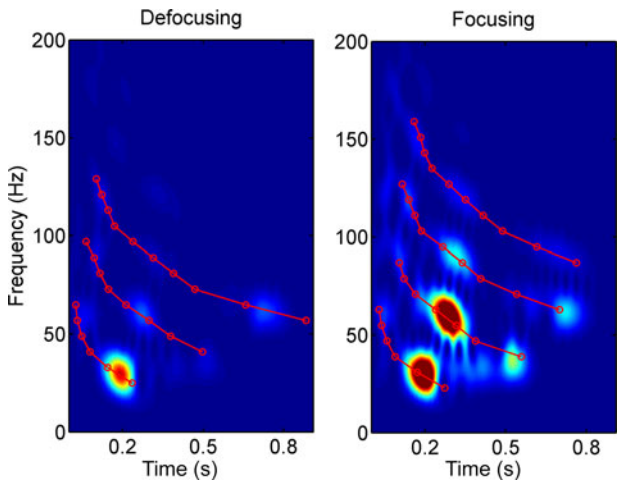

Fig. 6. Spectrogram and the extracted dispersion curves of the received signal on the bottom most hydrophone for a defocusing event at 19:25:00 (left) and a focusing event at 19:31:00 (right). The same color scale is used for both plots, and warm color represents large value.

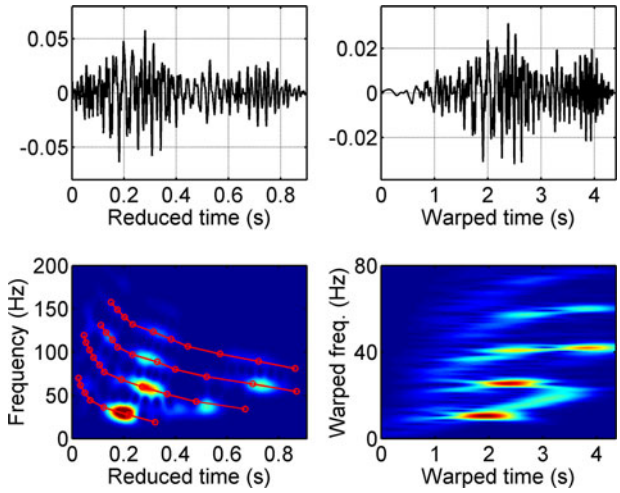

Fig. 7. Warping transform of the focusing event at 19:31:00 presented in the right panel of Fig. 6. (Upper left) The original signal. (Upper right) The warped signal. (Bottom right) Spectrogram of the warped signal. (Bottom left) Spectrogram of the original signal and extracted dispersion curves with samples shown by the red circles. Warm color represents large value for the plots in the bottom panels.

bottom and subsequently have effects on the results of geoacoustic inversion. This will be discussed in Section IV.

To separate the modes and extract mode spectra and dispersion curves of group speed, a modal filtering technique, the time-warping transform [19], was applied to single hydrophone data. The warped signal $y_w(t)$ is obtained by the time-warping transform on a given signal $y(t)$

$$y_{\mathrm{w}}(\mathrm{t}) = \sqrt{|\mathrm{w}'(\mathrm{t})|}\mathrm{y}[\mathrm{w}(\mathrm{t})] \tag{1}$$

where $\mathrm{w}(t)$ is the warping function and $\mathrm{w}\prime(t)$ is the derivative of $\mathrm{w}(t)$. The warping function is defined as

$$\mathrm{w}(t) = \sqrt{t^2 + t_r^2}, \qquad t_r = r/c_{\mathrm{w}} \tag{2}$$

where r is the source–receiver distance and c_{w} is the water sound speed. The warping transform is invertible. The transformation is adapted to an ideal isospeed waveguide with a rigid bottom. However, it is robust

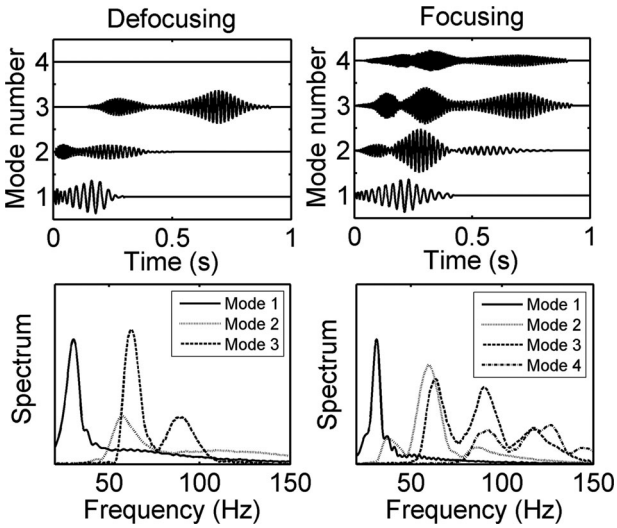

Fig. 8. Extracted mode signal (upper) and spectrum (bottom, solid, dashed, dotted and dash–dot curves represent modes 1, 2, 3, and 4, respectively) of the defocusing (left) and focusing (right) events presented in Fig. 6. The same scale is used for mode signals and the spectra, respectively.

to lack of detailed information about the sound channel and can be applied to most low-frequency shallow-water scenarios [20], [21]. By applying this transform to single hydrophone data dispersed modes can be extracted.

Fig. 7 illustrates the application of the warping transform for the focusing event at 19:31:00 presented in the right panel of Fig. 6. The received signal (upper left) is transformed to a warped signal (upper right). Its representation in the warped time-frequency domain is shown in the bottom-right panel where the warped modes are separated. The resolved modes are then filtered and unwarped to the original time domain using $\mathrm{w}^{-1}(t)$ to obtain the mode spectra and dispersion curves [21]. The arrival time is obtained by the known source–receiver distance and the extracted group speed. The spectrogram of the original signal is shown in the bottom-left panel. For this focusing event four modes were extracted that cover the frequency band 20–160 Hz. The same procedure was applied to the defocusing event at 19:25:00 presented in the left panel of Fig. 6. Only three modes were extracted in the frequency band 20–130 Hz. The extracted dispersion curves for the defocusing and focusing events are shown in Fig. 6 by the circles. Fig. 8 plots the separated mode signal (upper panels) and the spectrum (bottom panels, solid, dashed, dotted and dash–dot curves representing modes 1, 2, 3, and 4, respectively) of the defocusing (left) and focusing (right) events presented in Fig. 6. This procedure was applied to all of the defocusing and focusing events to extract dispersion curves. The estimated dispersion curves for all of the selected defocusing and focusing events are used as input for geoacoustic inversion to estimate the seabed parameters. Comparing the spectral amplitudes between the defocusing (bottom left) and focusing (bottom right) events in Fig. 8, mode 1 is not significantly affected by the internal wave, while mode 2 is influenced most by the internal wave. This is also observed at hydrophones at other depths, so it seems that the internal wave selectively affects mode 2. The reason could be that mode 2 has larger amplitude at shallower depths where the internal wave has large effect.

It is noted that there are uncertainties when extracting the dispersion curves since the warping transform involves manual operation. Due to the influence of internal waves the waveguide is distorted and the modes of the warped signal are not fully separated as shown in the bottom-right panel of Fig. 7 where modes 1 and 2 interfere with each other. To separate them and resolve each single mode, a mask function

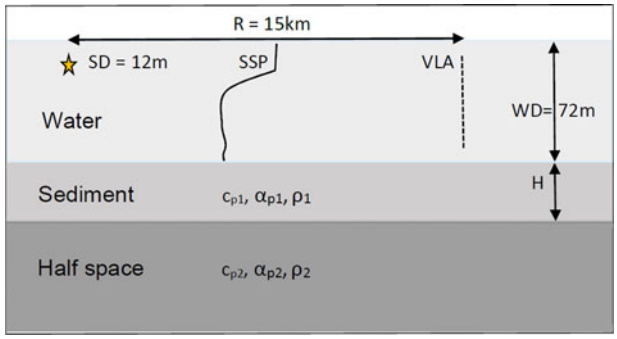

Fig. 9. Single sediment layer over half-space geoacoustic model.

on the spectrogram of the warped signal is applied. This operation introduces uncertainty in cutoff frequency, frequency coverage, and the allocation of energy between modes 1 and 2 in this event. Resampling also introduces uncertainty in cutoff and maximum frequencies. Denser sampling can reduce some of the uncertainty, but computation time increases. Uncertainties in the modal cutoff frequency and the frequency band affect the inferred penetration depth of the signal, and will influence the estimates of the sediment sound speed and the thickness in the inversion.

IV. Inversion Algorithm and Discussion of Inversion Results

A. Inversion Algorithm

The inversion is based on modal arrival times for each frequency component. The estimation for parameter vector $\mathbf{m}$ consisting of seabed parameters is given by

$$\mathbf{m} = \min_{\mathbf{m}} \left\{ \sum_{m,n=1}^{N_m, N_f} \left[\hat{t}_m(f_n) - dt - \hat{t}_m(f_n, \mathbf{m}) \right]^2 \right\} \tag{3}$$

where N_m is the number of modes, N_f is the number of frequencies, $\hat{t}_m(f_n)$ is the modal arrival time obtained from the estimated dispersion curves of group speed with the known source–receiver distance and a reference value of the water sound speed, $\hat{t}_m(f_n, \mathbf{m})$ is the predicted modal arrival time, and dt is a scalar introduced in the inversion for the correction of source emission time. The value of the parameter vector $\mathbf{m}$ minimizes the mean square error between the estimated and predicted modal arrival time of each mode. An optimization algorithm, adaptive simplex simulated annealing (ASSA) [22], is used in the inversion to obtain optimal estimates. In Section IV-B, this inversion scheme will be used to invert the estimated dispersion curves for the seven defocusing and seven focusing events to estimate seabed parameters, and the influence of acoustic frequency and number of modes on the inversion results is discussed.

B. Inversion Results and Discussion

Due to the small variation of the bathymetry along the acoustic propagation track, a range-independent geoacoustic model is assumed, a one-layer over half-space model as shown in Fig. 9. The geoacoustic parameters are sound speed, density, and attenuation in both the sediment and half-space, and the sediment thickness. Among these parameters only the sediment sound speed c_{p1}, thickness H, and density ρ_1 are set as estimated parameters, whereas other parameters including attenuation in the sediment layer and geoacoustic parameters in the substrate are assumed known since they are insensitive to modal arrival times. These parameters are chosen based on the preexisting "ground

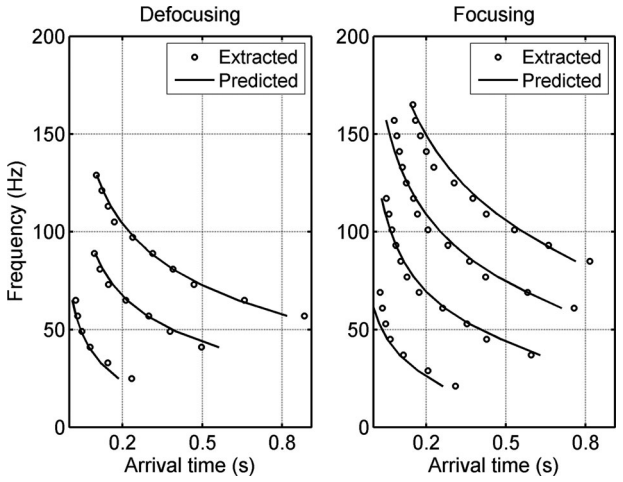

Fig. 10. Dispersion curves for the defocusing (left) and focusing (right) events shown in Fig. 6. The circles are the extracted dispersion curves shown in Fig. 6 and the solid curves are predicted from the inversion using ASSA optimization.

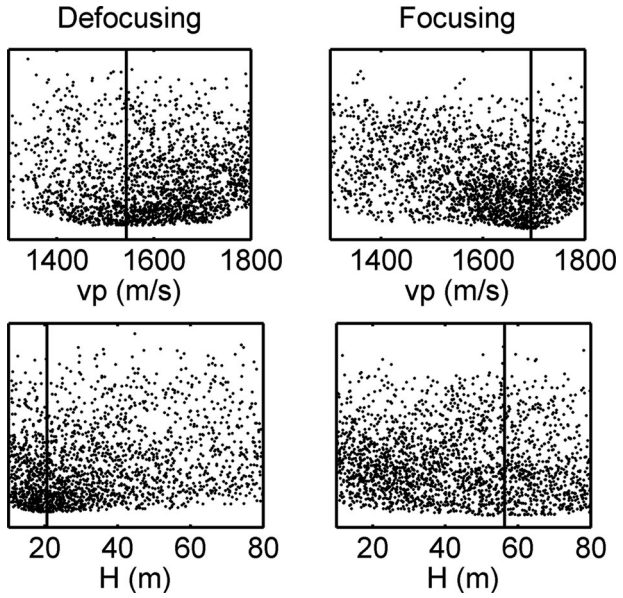

Fig. 11. Sensitivity plots of the sediment sound speed (upper) and the thickness (bottom) for the defocusing (left) and focusing (right) events shown in Fig. 6. The vertical line indicates the estimated value of each parameter. The range of abscissa values for each parameter indicates the search interval.

truth" information of the New Jersey continental shelf near the experimental site of SWARM'95 cited in [23] and the estimated values in [23]. The scalar dt, as described in Section IV-A, is also included as an estimated parameter.

Fig. 10 presents the extracted dispersion curves (circles) and the predicted dispersion curves (solid lines) using ASSA optimization for the events presented in Fig. 6. For both events, the predicted dispersion curves agree very well with the extracted dispersion curves at all frequencies, except at the cutoff frequencies. The inversion results indicate that dt is the most sensitive parameter, with a decreasing hierarchy of sensitivity to the sediment sound speeds, layer thickness, and density.

The sediment sound speed and the thickness are the most interesting parameters and their sensitivity analyses are plotted in Fig. 11 for the events presented in Fig. 6. The plots show the mismatch as a function of each estimated parameter and the optimal values indicated by the vertical lines. The sediment sound speed is sensitive, whereas the sediment thickness is less sensitive. The inversion was applied to all of the defocusing and focusing events in the selected time period, and the inversion results show that the sensitivities of the estimated parameters have similar patterns for each type of event.

TABLE I
INVERSION RESULTS OF THE DEFOCUSING EVENTS

Params. / Event	c_{p1} (m/s)	H (m)	ρ_1 (kg/m^3) *10^3	dt (s)
W1161	1575	26.8	1.15	-0.103
W1162	1530	19.6	1.03	-0.091
W1163	1431	12.3	1.05	-0.085
W1164	1380	20.6	2.30	-0.086
W1165	1543	20.6	1.31	-0.074
W1166	1518	23.7	1.35	-0.077
W1167	1445	18.9	1.54	-0.081
Mean	1489	20.4	1.39	-0.085
Std.	65.5	4.14	4.10	0.009

TABLE II
INVERSION RESULTS OF THE FOCUSING EVENTS

Params. / Event	c_{p1} (m/s)	H (m)	ρ_1 (kg/m^3) *10^3	dt (s)
W1168	1690	46.8	1.05	-0.109
W1169	1631	35.5	1.22	-0.102
W1170	1716	63.3	1.03	-0.132
W1171	1694	56.3	1.10	-0.115
W1172	1667	48.6	1.13	-0.123
W1173	1679	66.4	1.09	-0.122
W1174	1665	64.5	1.07	-0.106
Mean	1677	54.5	1.10	-0.116
Std.	24.9	10.5	0.60	0.010

The inversion results for the seven defocusing and seven focusing events are listed in Tables I and II, which give the overview of the inversion results of the estimated parameters. The estimated sediment sound speed and the thickness for the defocusing events are all smaller than those for the focusing events. The variation of the estimated sediment sound speeds within the defocusing events is larger than that within the focusing events. The mean and standard deviation are 1489 and 65.5 m/s for the defocusing events and 1677 and 24.9 m/s for the focusing events, respectively. The variation of the estimated sediment thickness within the defocusing event is smaller than that within the focusing events. The mean and standard deviation are 20.4 and 4.14 m for the defocusing events and 54.5 and 10.5 m for the focusing events, respectively.

Figs. 12 and 13 show the histograms of the inversion results of the sediment sound speed and the thickness for the defocusing (upper) and focusing (bottom) events with the means (the vertical lines). The sediment sound speed is narrowly distributed for the focusing events compared with that for the defocusing events, and there is no overlap

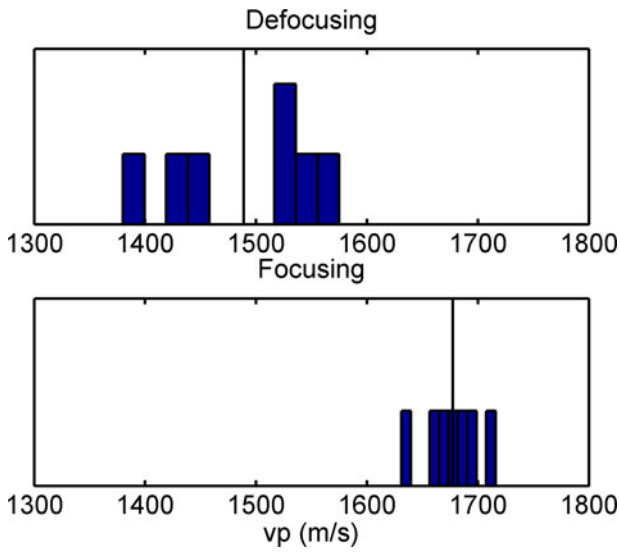

Fig. 12. Histogram of the inversion results listed in Tables I and II for the sediment sound speed and the mean (the vertical line). (Top) Defocusing events. (Bottom) Focusing events.

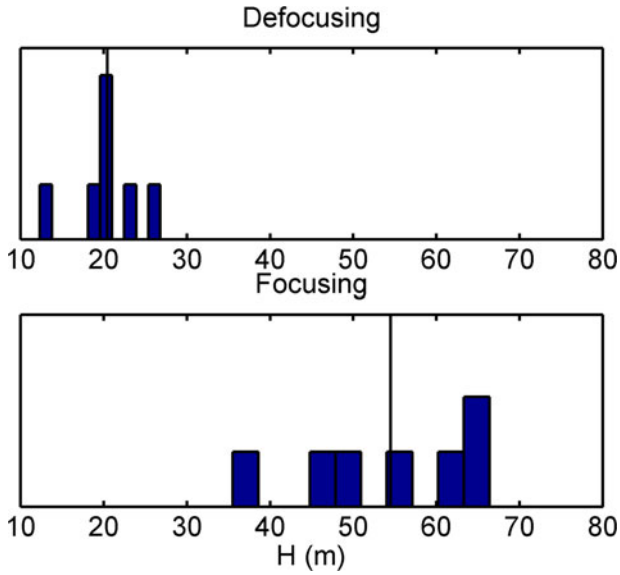

Fig. 13. Histogram of the inversion results listed in Tables I and II for the sediment thickness and the mean (the vertical line). (Top) Defocusing events. (Bottom) Focusing events.

between the inversion results of each type. For the sediment thickness there is no overlap in the distributions of estimated values between the inversions of each type of event.

The differences in the inversion results for the two types of events are due to the different number of modes and frequency bands used in the inversion, and the sound speed in the water column for the two different types of events. However, the most significant impacts are due to the number of modes and the frequency band of each mode, not modal arrival times that have a relatively small effect on the inversion results. To demonstrate this, the inversion procedure was repeated for the focusing events with only three modes in three cases: 1) keeping the frequency band unchanged; 2) changing the frequency band to the maximum frequency band among the modes of the defocusing events; 3) changing the frequency band as the smallest frequency band of each mode among the defocusing events. The inversion results (not listed in Tables) for case 1) indicate that the sediment sound speed and the thickness become relatively smaller than the estimated values with four modes. The amount of the difference depends on the frequency band of mode 4. The histograms (not plotted in figures) of the sediment sound speed and the thickness are still in the same regime as for the focusing events with four modes, and there is no overlap with the results for the defocusing events. The histograms of the sediment sound speed and the thickness for case 2) are shifted toward the estimated values of the defocusing events and there is some overlap for the sediment thickness with the results for the defocusing events. However, there is still some overlap for both the sediment sound speed and the thickness with the results for the focusing events with four modes. The sediment sound speed and the thickness of the inversion results for case 3) become similar with the results for the defocusing events, and the histograms of the sediment sound speed and the thickness for this case are shifted within the regime as for the defocusing events. Thus, the differences between the focusing and defocusing events are removed and the inversion results are more or less the same. The conclusion from the tests that were carried out is that the number of modes and the acoustic frequency band are significant factors that influence the inversion results. Although the modal arrival times are changed due to the differences in the water sound-speed profile, their impact on the inversion results does not appear to be large, perhaps because the changes in the lower order modes are relatively small.

A further remark is that the inversion results for the defocusing events are not reliable. The inversion results for the focusing events are close to the preexisting "ground truth" cited in [23] and the estimated results in [23]. This could be explained by considering that the modal structures for the focusing events are similar with those in the absence of internal waves. However, this may not be true for other data sets since there were no measured data without influence of the internal waves available for analysis and comparison.

V. Summary

In this paper, the influence of internal waves on sound propagation, modal behavior, and dispersion curves is studied by analysis of the broadband airgun data. The results of the analysis indicate that the variation in the sound propagation environment has a strong impact on the modal behavior and dispersion structure. The subsequent effects on the estimation of geoacoustic parameters are investigated by inverting arrival times of the dispersed modes from 14 data sets within a cycle of the sound intensity fluctuation (seven data sets for each type: defocusing and focusing) caused by internal waves. The inversion results for the events within each type are similar with a small standard deviation from the mean. However, the mean values and standard deviations between the defocusing and focusing types are quite different. The distributions of the inversion results between the two types have no overlap. The analysis and the inversion results have demonstrated that the number of modes and the acoustic frequency band of each mode are the most important factors to cause changes in the estimated sediment sound speed and the thickness, while the differences in the water sound speed in the upper part of the water column between defocusing and focusing events have little influence on the estimated changes in the sediment properties. The study in this paper indicates that detailed information and analysis of the conditions in propagation environment are crucial for doing geoacoustic inversion and obtaining reliable results. This might be also true for other inversion methods when using frequency and amplitude information for inversion since the internal waves change frequency and amplitude information as presented in this paper.

REFERENCES

[1] J. X. Zhou, X. Z. Zhang, and P. H. Rogers, "Resonant interaction of sound wave with internal solitons in the coastal zone," *J. Acoust. Soc. Amer.*, vol. 90, pp. 2042–2054, 1991.

[2] X. Z. Zhang and P. H. Rogers, "Modal characteristics of acoustic signal fluctuations induced by shallow water internal waves," in *Proc. MTS/IEEE OCEANS Conf.*, 1996, vol. 1, DOI: 10.1109/OCEANS.1996.572431.

[3] T. Duda and J. Preisig, "A modeling study of acoustic propagation through moving shallow water solitary wave packets," *IEEE J. Ocean. Eng.*, vol. 24, pp. 16–32, 1999.

[4] J. C. Preisig and T. F. Duda, "Coupled acoustic mode propagation through continental-shelf internal solitary waves," *IEEE J. Ocean. Eng.*, vol. 22, pp. 256–269, 1997.

[5] M. Badiey, Y. Mu, J. Lynch, J. Apel, and S. Wolf, "Temporal and azimuthal dependence of sound propagation in shallow water with internal waves," *IEEE J. Ocean Eng.*, vol. 27, no. 1, pp. 117–129, Jan. 2002.

[6] M. Badiey, B. Katsnelson, J. Lynch, S. Pereselkov, and W. Siegmann, "Measurement and modeling of 3-D sound intensity variations due to shallow water internal waves," *J. Acoust. Soc. Amer.*, vol. 117, no. 2, pp. 613–625, 2005.

[7] S. H. Weinberg and R. Burridge, "Horizontal ray theory for ocean acoustics," *J. Acoust. Soc. Amer.*, vol. 55, no. 1, pp. 63–79, 1974.

[8] S. D. Frank, M. Badiey, J. Lynch, and W. Siegmann, "Analysis and modeling of broadband airgun data influenced by nonlinear internal waves," *J. Acoust. Soc. Amer.*, vol. 116, no. 6, pp. 3404–3422, 2004.

[9] S. D. Frank, M. Badiey, and W. Siegmann, "Experimental evidence of three-dimensional acoustic propagation caused by nonlinear internal waves," *J. Acoust. Soc. Amer.*, vol. 118, no. 2, pp. 723–734, 2005.

[10] B. G. Katsnelson and S. Pereselkov, "Low-frequency horizontal acoustic refraction caused by internal wave solitons in a shallow sea," *Acoust. Phys.*, vol. 46, no. 6, pp. 684–691, 2000.

[11] B. G. Katsnelson and S. Pereselkov, "Space-frequency dependence of the horizontal structure of the sound field in the presence of intense internal waves," *Acoust. Phys.*, vol. 50, no. 2, pp. 169–176, 2004.

[12] M. Badiey, B. Katsnelson, J. Lynch and S. Pereselkov, "Frequency dependency and intensity fluctuations due to shallow water internal waves," *J. Acoust. Soc. Amer.*, vol. 122, no. 2, pp. 747–760, 2007.

[13] Y. Lin, C. Chen, and J. Lynch, "An equivalent transform method for evaluating the effect of water-column mismatch on geoacoustic inversion," *IEEE J. Ocean Eng.*, vol. 31, no. 2, pp. 284–298, 2006.

[14] K. M. Becker and G. V. Frisk, "The impact of water column variability on horizontal wave number estimation and mode based geoacoustic inversion results," *J. Acoust. Soc. Amer.*, vol. 132, no. 2, pp. 658–666, 2008.

[15] Y. Jiang and N. R. Chapman, "The impact of ocean sound speed variability on the uncertainty of geoacoustic parameter estimates," *J. Acoust. Soc. Amer.*, vol. 125, no. 5, pp. 2881–2895, 2009.

[16] H. Dong, M. Badiey, and N. R. Chapman, "Time-frequency analysis and modal behavior from airgun signals in shallow water," in *Proc. Inst. Acoust., Seabed Sediment Acoust.*, Univ. Bath, Bath, U.K., 2015, vol. 37, Pt. 1, pp. 1–6.

[17] C. F. Huang, P. Gerstoft, and W. S. Hodkiss, "Effect of ocean sound speed uncertainty on matched-field geoacoustic inversion," *J. Acoust. Soc. Amer.*, vol. 123, pp. EL162–EL168, 2008.

[18] M. S. Ballard and K. M. Becker, "Inversion for range-dependent water column sound speed profiles on the New Jersey shelf using a linearized perturbative method," *J. Acoust. Soc. Amer.*, vol. 127, no. 6, pp. 3411–3421, 2010.

[19] J. Bonnel and N. R. Chapman, "Geoacoustic inversion in a dispersive waveguide using warping operators," *J. Acoust. Soc. Amer.*, vol. 130, pp. EL101–EL107, 2011.

[20] J. Bonnel, B. Nicolas, J. Mars, and S. Walker, "Estimation of modal group velocities with a single receiver for geoacoustic inversion in shallow water," *J. Acoust. Soc. Amer.*, vol. 128, no. 2, pp. 719–727, 2010.

[21] J. Bonnel, C. Gervaise, P. Roux, B. Nicolas, and J. Mars, "Modal depth function estimation using time-frequency analysis," *J. Acoust. Soc. Amer.*, vol. 130, no. 1, pp. 61–71, 2011.

[22] S. Dosso, M. Wilmut, and A. Lapinski, "An adaptive-hybrid algorithm for geoacoustic inversion," *IEEE J. Ocean. Eng.*, vol. 26, no. 3, pp. 324–336, 2001.

[23] Y. Jiang, N. R. Chapman and M. Badiey, "Quantifying the uncertainty of geoacoustic parameter estimates for the New Jersey shelf by inverting air gun data," *J. Acoust. Soc. Amer.*, vol. 121, no. 4, pp. 1879–1894, 2007.

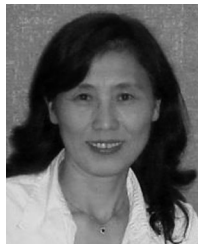

Hefeng Dong received the Ph.D. degree in geoacoustics from Jilin University, Changchun, China, in 1994.

She was a lecturer from 1986 to 1994 and an Associate Professor from 1995 to 2000 at the Department of Physics, Northeast Normal University, Changchun, China. She was a visiting scholar and Postdoctorial Fellow at the Norwegian University of Science and Technology, Trondheim, Norway, from 1999 to 2000 and from 2000 to 2001. She was a Research Scientist at the SINTEF Petroleum Research, Trondheim, Norway, between 2001 and 2002. Since 2002, she has been a Professor with the Norwegian University of Science and Technology. Between 2008 and 2009, she was a Visiting Professor with the Underwater Acoustics Laboratory, University of Victoria, Victoria, BC, Canada. Between 2014 and 2015, she was on one-year sabbatical as a visiting scientist with the College of Earth, Ocean, and Environment, University of Delaware, Newark, DE, USA. Her research interests include wave propagation modeling, geoacoustic inversion, and signal processing in ocean acoustics and underwater acoustic communication.

Dr. Dong is a member of the Acoustical Society of America.

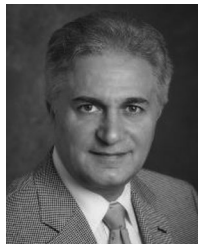

Mohsen Badiey (M'94) received the Ph.D. degree in applied marine physics and ocean engineering from the Rosenstiel School of Marine and Atmospheric Science, University of Miami, Miami, FL, USA, in 1988.

He was a Postdoctoral Fellow at the Port and Harbour Institute, Ministry of Transport, Tokyo, Japan, from 1988 through 1990, and worked on research problems related to the water–wave interaction with seafloor and on seismic wave propagation in continental shelf regions. In 1990, he became a faculty member at the College of Earth, Ocean, and Environment, University of Delaware, Newark, DE, USA, where he is currently a full Professor in the Physical Ocean Science and Engineering Program and in the Civil Engineering Department. From 1992 to 1995, he managed the ocean acoustics program at the U.S. Office of Naval Research. His research interests are physics of sound and vibration, underwater acoustics in shallow-water regions, acoustical oceanography, underwater acoustic communications, seabed acoustics, and geophysics.

Dr. Badiey is a Fellow of the Acoustical Society of America.

N. Ross Chapman (M'97–SM'03–F'10) received the Ph.D. degree in physics from the University of British Columbia, Vancouver, BC, Canada, in 1975.

He is Emeritus Professor, recently retired from the University of Victoria, Victoria, BC, Canada, following a career of over 35 years in underwater acoustics, signal processing, and acoustical oceanography. He worked for Defence Research in Canada as Leader of the Ocean Acoustics Group (1976–1995), before moving on to the University of Victoria as a Research Chair in Ocean Acoustics, and Director of the Centre for Earth and Ocean Sciences at the University of Victoria (2000–2006). He continues to maintain his research interests in ocean acoustic propagation and modeling, advanced signal processing, ocean ambient noise measurement and modeling, and inversion of ocean seabed properties from acoustic field data.

Prof. Chapman is an elected Fellow of the Acoustical Society of America, and is the Editor-in-Chief of the IEEE JOURNAL OF OCEANIC ENGINEERING.